20th AIAA Computational Fluid Dynamics Conference
27 - 30 June 2011, Honolulu, Hawaii

AIAA 2011-3227

A $P_N P_M$-CPR Framework for Hyperbolic Conservation Laws

Z.J. Wang[1] and Lei Shi[2]
Department of Aerospace Engineering and CFD Center, Iowa State University, Ames, IA, 50011

Song Fu[3]
Department of Engineering Mechanics, Tsinghua University, Beijing, China, 100084

Hanxin Zhang[4]
National Laboratory for Computational Fluid Dynamics, Beijing, China, 100083

and

Laiping Zhang[5]
State Key Laboratory of Aerodynamics, Mianyang, Sichuan, China, 621000

The $P_N P_M$ or reconstructed discontinuous Galerkin method is a hybrid finite volume and discontinuous Galerkin method, in which neighboring cells are used to reconstruct a higher order polynomial than the solution representation in the cell under consideration. The CPR method is a discontinuous nodal formulation unifying several well-known methods in a simple finite difference like manner. In this paper, we present several $P_N P_M$ schemes under the CPR framework. Many interesting schemes with various orders of accuracy and efficiency are developed. Their performance is illustrated with several benchmark test cases.

I. Introduction

MOST production CFD codes used in the aerospace industry is either first or second order accurate. This means that the solution error is proportional to h or h^2, with h being the mesh size. Numerical methods of 1st and 2nd order accuracy are called low order methods conventionally, while 3rd and higher order ones are defined as high-order methods in the aerospace community. For 3D simulations, if the mesh resolution is doubled in both space and time, the computational cost increases by a factor of 16, but the solution error only decreases by a factor of 2 with a 1st order scheme and a factor of 4 with a 2nd order scheme. On the other hand, the solution error with a 6th order scheme decreases by a factor of 64 with a 16 fold increase in computational cost when resolution doubles. Obviously, if high accuracy is required, low order methods are not as efficient as high order methods with grid refinement.

Because of the potential of high accuracy and efficiency, high-order methods have received considerable research interest in the global CFD community in the last two decade. A variety of high order methods have been developed. Refer to several books [18,13,35] and reviews [9,34] for the state-of-the-art and recent progresses in the development of such methods.

Most high order methods employ polynomials of degree 2 or higher to approximate the (unknown) solution. In two dimensions, at least six degrees of freedom (DOFs) or solution unknowns are required to build a degree 2 polynomial. Depending on how many DOFs are available on a cell or element, multiple cells may be needed to build the solution polynomial. For example, at least 5 neighboring cells are required to build a degree 2 polynomial in a finite volume method because each cell only has one DOF, the cell-averaged solution. In a discontinuous Galerkin (DG) [2-6,10,25-26,32,39], residual distribution (RD) [1], spectral volume (SV) [21,33,38] /difference (SD) [19,22,24,30] or the

[1] Wilson Professor of Engineering, Department of Aerospace Engineering and CFD Center, 2271 Howe Hall, Associate Fellow of AIAA.
[2] PhD Student, Department of Aerospace Engineering and CFD Center, 2271 Howe Hall.
[3] Professor, Department of Engineering Mechanics. Senior Member AIAA.
[4] Academician of Chinese Academy of Sciences, National Laboratory for Computational Fluid Dynamics.
[5] Professor, State Key Laboratory of Aerodynamics.

correction procedure via reconstruction (CPR) method [14-17,36-37], each cell has enough DOFs so that neighboring data is not required in building the solution polynomial. Such methods are compact because only immediate face neighbors play a role in updating the DOFs in the current cell. Compact methods are easy to implement on CPU and GPU clusters, and highly scalable because the amount of data communication is relatively small.

Although 2nd order finite volume schemes are not strictly compact as neighbor's neighbors are used in the solution update, they can be implemented in a "compact" manner by messaging passing through only immediate neighbors on a parallel computer. This is because the reconstruction stencil is compact as shown in Figure 1, which shows both the "reconstruction stencil" and the "scheme stencil".

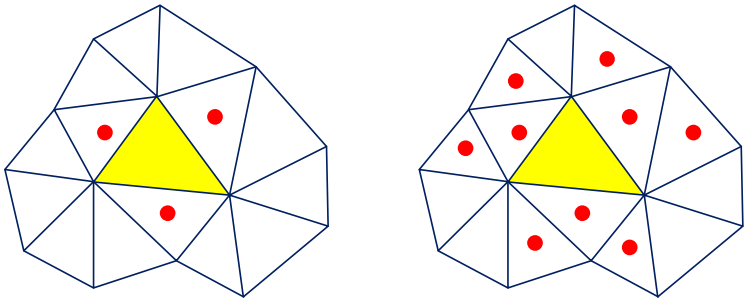

(a) Reconstruction stencil (a) Scheme stencil

Figure 1. Illustration of the reconstruction and scheme stencils

More recently, hybrid methods named P_NP_M [7-8], reconstructed DG (RDG) [23], hybrid FV/DG [41], weighted integral based schemes[40] have been developed. The key idea of these methods is to use multiple DOFs on the current cell and its neighbors to build a solution polynomial higher than that with the DOFs on a single element. This solution polynomial is then used to generate high-order updates for the DOFs on the current element. This hybrid approach thus offers a whole new host of possibilities:

- How to reconstruct the solution polynomial and at what degree?
- How to update the DOFs at the current element?

The number of choices is quite large, and in fact, the FV and DG/SV/SD/CPR methods can be viewed as two extreme special cases of the new family of possible methods. As mentioned earlier, many choices have already been explored, and some unique features have been demonstrated, e.g.,

- More efficient per DOF than either the FV or DG method;
- Lower memory requirement for implicit schemes to achieve a given order of accuracy than the DG method.

In the present study, we test the hybrid approach in the context of CPR, a finite difference-like nodal formulation [14-17,36-37]. We attempt to maintain the simplicity in the formulation, while investigating the accuracy and stability of different choices. In the next section, we briefly review the CPR approach. In Section III, the basic P_NP_M-CPR formulation will be described in both 1D and 2D. Numerical results are presented in Section IV for the Euler equations, and conclusions are given in Section V.

II. Review of the CPR Formulation

For the sake of completeness, the CPR formulation is briefly reviewed. The CPR formulation was originally developed by Huynh in [15-16] under the name of flux reconstruction, and extended to simplex and hybrid elements by Wang & Gao in [35] under lifting collocation penalty. The authors later decided to employ the unified name CPR for the method. In [14], CPR was further extended to 3D hybrid meshes. The method is also described in two book chapters [35]. CPR can be derived from a weighted residual method by transforming the integral formulation into a differential one. First, a hyperbolic conservation law can be written as

$$\frac{\partial Q}{\partial t} + \vec{\nabla} \bullet \vec{F}(Q) = 0, \tag{1}$$

with proper initial and boundary conditions, where Q is the state vector, and $\vec{F} = (F, G)$ is the flux vector. Assume that the computational domain Ω is discretized into N non-overlapping triangular elements $\{V_i\}_{i=1}^{N}$. Let W be an arbitrary weighting function or test function. The weighted residual formulation of (1) on element V_i can be expressed as

$$\int_{V_i}\left(\frac{\partial Q}{\partial t}+\vec{\nabla}\bullet\vec{F}(Q)\right)WdV=\int_{V_i}\frac{\partial Q}{\partial t}WdV+\int_{\partial V_i}W\vec{F}(Q)\bullet\vec{n}\,dS-\int_{V_i}\vec{\nabla}W\bullet\vec{F}(Q)dV=0. \tag{2}$$

Let Q_i be an approximate solution to the analytical solution Q on V_i. On each element, the solution belongs to the space of polynomials of degree *k* or less, i.e., $Q_i \in P^k(V_i)$ (or P^k if there is no confusion) with no continuity requirement across element interfaces. Let the dimension of P^k be *K = (k+1)(k+2)/2*. In addition, the numerical solution Q_i, for the moment, is required to satisfy (2)

$$\int_{V_i}\frac{\partial Q_i}{\partial t}WdV+\int_{\partial V_i}W\vec{F}(Q_i)\bullet\vec{n}\,dS-\int_{V_i}\vec{\nabla}W\bullet\vec{F}(Q_i)dV=0. \tag{3}$$

Obviously the surface integral is not properly defined because the numerical solution is discontinuous across element interfaces. Following the idea used in the Godunov method[11,31], the normal flux term in (3) is replaced with a common Riemann flux, e.g., in [20,27-28]

$$F^n(Q_i)\equiv\vec{F}(Q_i)\bullet\vec{n}\approx F^n_{com}(Q_i,Q_{i+},\vec{n}), \tag{4}$$

where Q_{i+} denotes the solution outside the current element V_i. Instead of (3), the approximate solution is required to satisfy

$$\int_{V_i}\frac{\partial Q_i}{\partial t}WdV+\int_{\partial V_i}WF^n_{com}dS-\int_{V_i}\vec{\nabla}W\bullet\vec{F}(Q_i)dV=0. \tag{5}$$

Applying integration by parts again to the last term of the above LHS, we obtain

$$\int_{V_i}\frac{\partial Q_i}{\partial t}WdV+\int_{V_i}W\vec{\nabla}\bullet\vec{F}(Q_i)dV+\int_{\partial V_i}W\left[F^n_{com}-F^n(Q_i)\right]dS=0. \tag{6}$$

Here, the test space has the same dimension as the solution space, and is chosen in a manner to guarantee the existence and uniqueness of the numerical solution.

Note that the quantity $\vec{\nabla}\bullet\vec{F}(Q_i)$ involves no influence from the data in the neighboring cells. The influence of these data is represented by the above boundary integral, which is also called a "penalty term", penalizing the normal flux differences.

The next step is critical in the elimination of the test function. The boundary integral above is cast as a volume integral via the introduction of a "correction field" on V_i, $\delta_i \in P^k(V_i)$,

$$\int_{V_i}W\delta_i dV=\int_{\partial V_i}W[F^n]dS, \tag{7}$$

where $[F^n]=F^n_{com}-F^n(Q_i)$ is the normal flux difference. The above equation is sometimes referred to as the "lifting operator", which has the normal flux differences on the boundary as input and a member of $P^k(V_i)$ as output. Substituting (7) into (6), we obtain

$$\int_{V_i}\left[\frac{\partial Q_i}{\partial t}+\vec{\nabla}\bullet\vec{F}(Q_i)+\delta_i\right]WdV=0. \tag{8}$$

If the flux vector is a linear function of the state variable, then $\vec{\nabla}\bullet\vec{F}(Q_i)\in P^k$. In this case, the terms inside the square bracket are all elements of P^k. Because the test space is selected to ensure a unique solution, Eq. (8) is equivalent to

$$\frac{\partial Q_i}{\partial t} + \vec{\nabla} \bullet \vec{F}(Q_i) + \delta_i = 0 \quad . \tag{9}$$

For nonlinear conservation laws, $\vec{\nabla} \bullet \vec{F}(Q_i)$ is usually not an element of P^k. As a result, (8) cannot be reduced to (9). In this case, the most obviously choice is to project $\vec{\nabla} \bullet \vec{F}(Q_i)$ into P^k. Denote $\Pi\left(\vec{\nabla} \bullet \vec{F}(Q_i)\right)$ a projection of $\vec{\nabla} \bullet \vec{F}(Q_i)$ to P^k. One choice is

$$\int_{V_i} \Pi\left(\vec{\nabla} \bullet \vec{F}(Q_i)\right) W dV = \int_{V_i} \vec{\nabla} \bullet \vec{F}(Q_i) W dV \quad . \tag{10}$$

Then (8) reduces to

$$\frac{\partial Q_i}{\partial t} + \Pi\left(\vec{\nabla} \bullet \vec{F}(Q_i)\right) + \delta_i = 0 \quad . \tag{11}$$

With the introduction of the correction field δ_i, and a projection of $\vec{\nabla} \bullet \vec{F}(Q_i)$ for nonlinear conservation laws, we have reduced the weighted residual formulation to a differential formulation, which involves no explicit integrals. Note that for δ_i defined by (7), if $W \in P^k$, Eq. (11) is equivalent to the DG formulation, at least for linear conservation laws; if W belongs to another space, the resulting δ_i is different. We obtain a formulation corresponding to a different method such as the SV method.

Next, let the DOFs be the solutions at a set of solution points (SPs) $\left\{\vec{r}_{i,j}\right\}$ (j varies from 1 to K), as shown in Figure 2. Then Eq. (11) holds true at the SPs, i.e.,

$$\frac{\partial Q_{i,j}}{\partial t} + \Pi_j\left(\vec{\nabla} \bullet \vec{F}(Q_i)\right) + \delta_{i,j} = 0 \quad , \tag{12}$$

where $\Pi_j\left(\vec{\nabla} \bullet \vec{F}(Q_i)\right)$ denotes the values of $\Pi\left(\vec{\nabla} \bullet \vec{F}(Q_i)\right)$ at SP j. The efficiency of the CPR approach hinges on how the correction field δ_i and the projection $\Pi\left(\vec{\nabla} \bullet \vec{F}(Q_i)\right)$ are computed. Two approaches can be used to compute this divergence as detailed in [36].

To compute δ_i, we define $k+1$ points named flux points (FPs) along each interface, where the normal flux differences are computed, as shown in Figure 2. We approximate (for nonlinear conservation laws) the normal flux difference $[F^n]$ with a degree k interpolation polynomial along each interface,

$$[F^n]_f \approx \mathbf{I}_k [F^n]_f \equiv \sum_l [F^n]_{f,l} L_l^{FP}, \tag{13}$$

where f is an face (or edge in 2D) index, and l is the FP index, and L_l^{FP} is the Lagrange interpolation polynomial based on the FPs in a local interface coordinate. For linear triangles with straight edges, once the solution points and flux points are chosen, the correction at the SPs can be written as

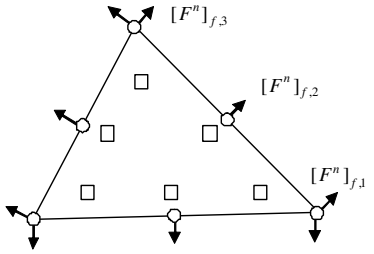

Figure 2. Solution points (squares) and flux points (circles) for k = 2

$$\delta_{i,j} = \frac{1}{|V_i|} \sum_{f \in \partial V_i} \sum_l \alpha_{j,f,l} [F^n]_{f,l} S_f, \tag{14}$$

where $\alpha_{j,f,l}$ are lifting constants independent of the solution, S_f is the face area, $|V_i|$ is the volume of V_i. Note that the correction for each solution point, namely $\delta_{i,j}$, is a linear combination of all the normal flux differences on

all the faces of the cell. Conversely, a normal flux difference at a flux point on a face, say (*f, l*) results in a correction at all solution points *j* of an amount $\alpha_{j,f,l}[F^n]_{f,l}S_f / |V_i|$.

For 1D conservation laws, Eq. (12) reduces to

$$\frac{\partial Q_{i,j}}{\partial t} + \Pi_j\left(\frac{\partial F(Q_i)}{\partial x}\right) + \frac{1}{h_i}\left(\alpha_{L,j}[F^n]_L + \alpha_{R,j}[F^n]_R\right) = 0, \tag{15}$$

where h_i is the length of element *i*, which has two interfaces, the left one and right one, with unit face "areas" and unit face "normals" of -1 and 1 respectively, so that $[F^n]_L = -[F]_L$, $[F^n]_R = [F]_R$, $\alpha_{L,j}$ and $\alpha_{R,j}$ are constant lifting coefficients in 1D. Due to symmetry, we have $\alpha_{L,j} = \alpha_{R,k+2-j}$. For the 1D case, details can be found in [15-17].

III. Hybrid P_NP_M -CPR Formulation

A. 1D Formulation

Let's start from the 1D conservation law to present the basic idea. Consider a 2nd order CPR formulation with two solution points (SPs) within each cell. In the most efficient CPR formulation, the two end points of the cell are used as the SPs (usually called the Lobatto points) since it is not necessary to reconstruct the solutions there for flux computation. Obviously interior points such as the Gauss points can also be used as the SPs as shown in Figure 3. In order to distinguish schemes based on these two types of SPs, P_NP_M-CPR-L is used to denote schemes based on the Labatto points, while P_NP_M-CPR-G is used to denote schemes based on the Gauss points. In a P_NP_M formulation, both the left and right cells are used in reconstructing a higher order polynomial, denoted as U_i (vs. Q_i, the polynomial defined based on DOFs at the current cell). We employ an interpolation based reconstruction approach for simplicity since the DOFs are nodal values at a given set of points. If the SPs are Lobatto points, multiple values exist at cell interfaces. Not all of them can be used in the reconstruction. As we always prefer local data, this means the interface solutions at the two neighboring cells are excluded in the reconstruction. Therefore the highest degree of U_i is 3 for P_1P_M -CPR-L schemes. But for P_1P_M-CPR-G schemes, the highest degree is 5 because solutions at all six solution points can be used in the reconstruction. The reconstruction stencils are shown in Figure 3 for both types of schemes. The reconstruction polynomial U_i is then used to generate high-order updates in the following fashion.

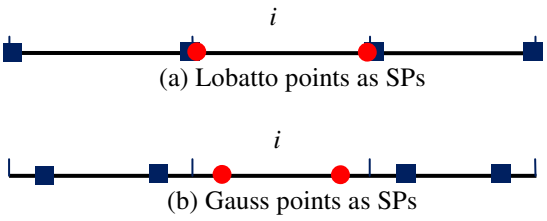

(a) Lobatto points as SPs

(b) Gauss points as SPs

Figure 3. Schematic of Labatto and Gauss points as the solution points

First it is used to compute the interior divergence term, i.e. $\frac{\partial F(U_i)}{\partial x}$. Next U_i is also used to compute the difference between the common flux and the interior flux, e.g., $[F^n]_L$ and $[F^n]_R$. The common Riemann flux is computed with the reconstruction polynomials at neighboring cells. For example, the common flux at interface i+1/2 is computed using

$$F_{i+1/2,com} = \hat{F}_{Riem}(U_i(x_{i+1/2}), U_{i+1}(x_{i+1/2})). \tag{16}$$

The interior flux is also computed with the reconstruction polynomial so that the flux difference is

$$\left[F^n\right]_R = \hat{F}_{Riem}(U_i(x_{i+1/2}), U_{i+1}(x_{i+1/2})) - F(U_i(x_{i+1/2})). \tag{17}$$

Finally the P_NP_M -CPR scheme is

$$\frac{\partial Q_{i,j}}{\partial t} + \Pi_j \left(\frac{\partial F(U_i)}{\partial x} \right) + \frac{1}{h_i} \left(\alpha_{L,j} [F^n]_L + \alpha_{R,j} [F^n]_R \right) = 0. \tag{18}$$

Note that the lifting coefficients ($\alpha_{L,j}, \alpha_{R,j}$) remain exactly the same. Obviously the hybrid scheme is uniquely defined once the reconstruction polynomial U_i is determined.

There are many choices on how U_i is reconstructed. For the sake of accuracy and stability, the following rules of thumb are established:

- The values of the reconstruction polynomial at the solution points are identical to the original solutions at the solution points, i.e.,

$$U_i(x_{i,j}) = Q_i(x_{i,j}), \tag{19}$$

  where $x_{i,j}$ denotes the *jth* solution point of cell *i*.
- The reconstruction stencil is symmetric with respect to cell *i*. This is because upwinding is provided by the Riemann flux so that a central reconstruction stencil is preferred for the sake of accuracy and stability.
- Nearby data is always preferred than far away data.
- A constrained least squares approach[7] is used when the number of DOFs on the reconstruction stencil is larger than the dimension of the polynomial space, e.g., if 6 solutions are available to reconstruct a degree 4 polynomial.

Based on the above rules, the P_NP_M-CPR-L schemes are expected to be more efficient than P_NP_M -CPR-G schemes since the interface flux difference term is exactly the same as the CPR schemes. The only difference is the flux divergence term. In order to evaluate the performance of the P_NP_M-CPR formulation, we test the following schemes:

1. *P_1P_3–CPR-L scheme*
   In this scheme, a unique degree 3 polynomial U_i is built using $\{Q_{i-1,1}, Q_{i,1}, Q_{i,2}, Q_{i+1,2}\}$.

2. *P_1P_3–CPR-G-I scheme*
   This scheme uses an "incomplete" stencil to build a degree 3 polynomial by excluding two solutions further away from the current cell. So the reconstruction stencil is $\{Q_{i-1,2}, Q_{i,1}, Q_{i,2}, Q_{i+1,1}\}$.

3. *P_1P_5–CPR-G-C scheme*
   This scheme uses the "complete" stencil to build the highest polynomial - a degree 5 polynomial. So the reconstruction stencil is $\{Q_{i-1,1}, Q_{i-1,2}, Q_{i,1}, Q_{i,2}, Q_{i+1,1}, Q_{i+1,2}\}$.

4. *P_1P_3–CPR-G-C scheme*
   This scheme uses the "complete" stencil to build a degree 3 polynomial using constrained least squares. The reconstruction stencil is the same as that of *P_1P_5–CPR-G-C*.

5. *P_1P_4–CPR-G-C scheme*
   This scheme uses the "complete" stencil to build a degree 4 polynomial using constrained least squares. The reconstruction stencil is the same as that of *P_1P_5–CPR-G-C*.

6. *P_2P_6–CPR-L scheme*
   In this scheme, a unique degree 6 polynomial U_i is built using $\{Q_{i-1,1}, Q_{i-1,2}, Q_{i,1}, Q_{i,2}, Q_{i,3}, Q_{i+1,2}, Q_{i+1,3}\}$.

7. *P_2P_4–CPR-G-I scheme*
   This scheme uses an "incomplete" stencil to build a degree 4 polynomial by including two nearby solutions from the neighboring cells. So the reconstruction stencil is $\{Q_{i-1,3}, Q_{i,1}, Q_{i,2}, Q_{i,3}, Q_{i+1,1}\}$.

8. *P_2P_6–CPR-G-I scheme*
   This scheme uses an "incomplete" stencil to build a degree 6 polynomial. So the reconstruction stencil is $\{Q_{i-1,2}, Q_{i-1,3}, Q_{i,1}, Q_{i,2}, Q_{i,3}, Q_{i+1,1}, Q_{i+1,2}\}$.

9. P_2P_8–CPR-G-C scheme

This scheme uses a "complete" stencil to build the highest polynomial - a degree 8 polynomial. All solutions from the neighboring cells are used in the reconstruction.

10. P_2P_6–CPR-G-C scheme

This scheme uses the "complete" stencil to build a degree 6 polynomial using constrained least squares.

The above schemes are tested in a grid refinement accuracy study using the following one dimensional linear wave equation:

$$\frac{\partial Q}{\partial t}+\frac{\partial Q}{\partial x}=0, \quad x\in[0,1] \tag{20}$$

with the initial condition $Q(x,0)=\sin(2\pi x)$, and periodic boundary conditions. The time integration schemes used are the TVD Runge–Kutta schemes of 3rd or 4th order accuracy[12]. The computation is carried out until t = 1. The L_2 error is plotted in Figure 4. and summarized in Table 1. Note that the hybrid P_NP_M-*CPR* formulation can significantly improve the order of accuracy of the original CPR schemes. The highest order of accuracy is 5th with the P_1P_M -*CPR* schemes and 8th with the P_2P_M -*CPR* schemes. The numeric tests indicate that the constrained least squares reconstruction is more stable than the conventional least squares method for the P_M reconstruction. When the number of data items in the P_M reconstruction stencil is more than the nDOFs needed for the higher-order polynomial, P_NP_M-*CPR* schemes with an incomplete stencil is more accurate than those with a complete stencil.

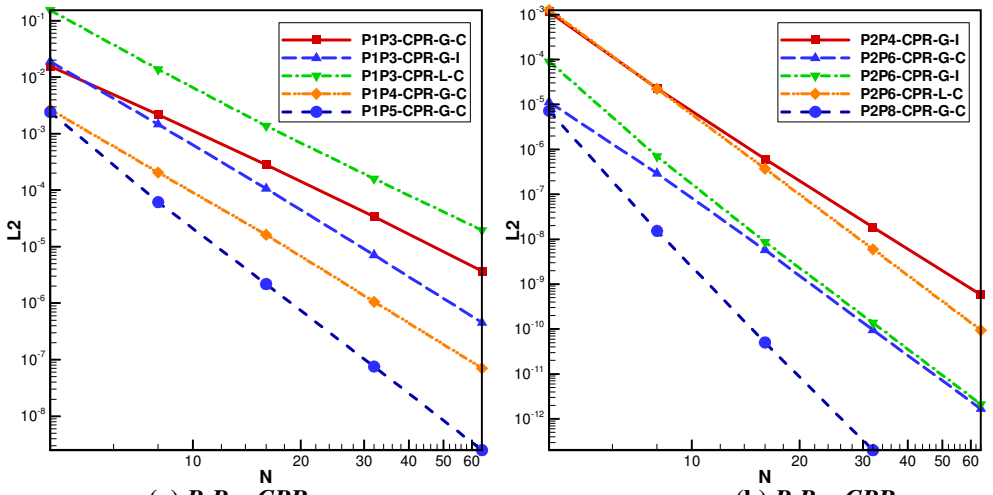

(a) P_1P_M–*CPR* **(b) P_2P_M–*CPR***

Figure 4. L_2 error of the (a) P_1P_M–*CPR* and (b) P_2P_M–*CPR* schemes for the 1D linear wave equation at t=1.

B. 2D Formulation for a simplex

The extension of the P_NP_M-*CPR* schemes to a simplex is similar to the 1D formulation and quite straightforward. Again we have two choices to distribute the solution points, as shown in Figure 5 in the case of N = 1. If Lobatto points are used in the interpolation based reconstruction, solutions at 6 unique locations can be used in the reconstruction, resulting in a degree 2 polynomial. The scheme is named a P_1P_2-*CPR-L* scheme. On the other hand, if the solution points are the Gauss points, none of the SPs coincide with each other. Thus all DOFs of the reconstruction stencil can be used for reconstructing the higher order polynomial U_i. Following the rules of thumb described earlier, we can design the following three schemes for N = 1:

1. *P_1P_3–CPR-G-C scheme*
   In this scheme, all DOFs in the stencil are used to reconstruct a degree 3 polynomial U_i using a constrained least squares approach.

2. *P_1P_2–CPR-G-C scheme*
   In this scheme, all DOFs in the stencil are used to reconstruct a degree 2 polynomial U_i using a constrained least squares approach.

3. *P_1P_2–CPR-G-I2 scheme*
   In this scheme, not all DOFs in the stencil are used in the reconstruction. Instead, only the nearest 6 DOFs from the three neighboring cells are selected and a constrained least squares approach is employed to build U_i. I2 stands for only the nearest 2 DOFs from each neighboring cell are used.

Once the higher-order polynomial is obtained, it is obviously used in computing the interior divergence term $\vec{\nabla}\bullet\vec{F}(U_i)$. There appear to be at least two options in how the correction terms are computed in multiple dimensions.

Option CN (Correction order N): The correction term is computed exactly in the same way as in the CPR approach with the same coefficients $\alpha_{j,f,l}$, and with the same number of flux points along each face. Therefore, no new points are added on the face. However, the flux difference is computed with the reconstruction polynomial U_i. For example, the common flux is computed using the reconstructed solutions on both sides of a face, and the interior flux is also computed with the reconstructed higher order polynomial at the current cell.

Option CM (Correction order M): The normal flux difference is assumed to be of order M along the face. As a result, extra flux points are added on the faces to support a degree M polynomial. Then new correction coefficients $\alpha_{j,f,l}$ are derived from the lifting operator given in Eq. 7. Obviously the reconstruction polynomial is used to compute the flux difference at all the flux points.

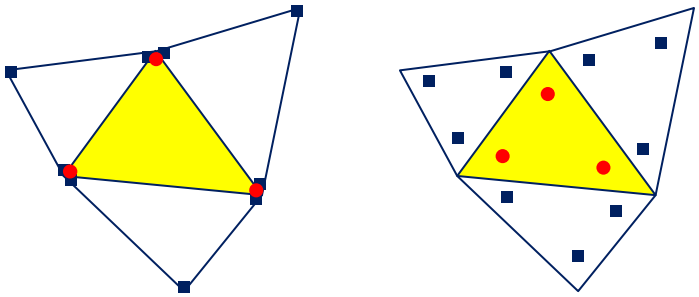

(a) Labatto points as SPs (b) Gauss points as SPs

Figure 5. Distribution of solution points for a simplex in 2D

In addition to the N = 1 schemes, the following P_2P_M schemes are also tested:

4. *P_2P_3–CPR-G-C scheme*
   In this scheme, all DOFs in the stencil are used to reconstruct a degree 3 polynomial U_i using a constrained least squares approach.

5. *P_2P_3–CPR-G-I3 scheme*

In this scheme, an "incomplete" stencil are used to reconstruct a degree 3 polynomial U_i by excluding three solutions further away from the current cell. I3 stands for only the nearest 3 DOFs from each neighboring cell are used.

6. *P_2P_3–CPR-L-C scheme*

In this scheme, all DOFs in the stencil are used to reconstruct a degree 3 polynomial U_i using a constrained least squares approach.

7. *P_2P_3–CPR-L-I2 scheme*

In this scheme, an "incomplete" stencil are used to reconstruct a degree 3 polynomial U_i by excluding one solution further away from the current cell. I2 stands for only the nearest 2 DOFs from each neighboring cell are used.

The above 2D schemes are tested with a 2D linear wave equation:

$$\frac{\partial Q}{\partial t}+\frac{\partial Q}{\partial x}+\frac{\partial Q}{\partial y}=0, \tag{21}$$

$$x\in[-1,1],\quad y\in[-1,1],\quad \text{perodic boundary condtions},$$

under the initial condition $Q(x,y,0)=\sin\pi(x+y)$. The computation is carried out until t = 1 on a set of irregular triangular mesh as shown in Figure 6. The L_2 errors are plotted in Figure 7 and summarized in Table 2. The results show that we get an extra order of accuracy with the *P_1P_M–CPR* and *P_2P_M–CPR* schemes. Due to the limited number of the available DOFs in the P_M reconstruction stencil, the simulations with the *P_1P_3–CPR-G-C* scheme and the *P_1P_2–CPR-G-I2* scheme are unstable. In order to enhance the robustness of the P_M reconstruction, we need to use more DOFs in P_M stencil than needed. For the same reason, the *P_NP_M-CPR* schemes with Gauss points is preferred over the schemes with Lobatto points. Note that with Lobatto points, a CN correction produces more stable and accurate schemes than a CM correction; while with Gauss points, a CM correction is more stable and accurate than a CN correction. We are now performing analysis to understand why this is the case. Note also that incomplete stencils are more accurate than the complete stencil. This is similar to the 1D test.

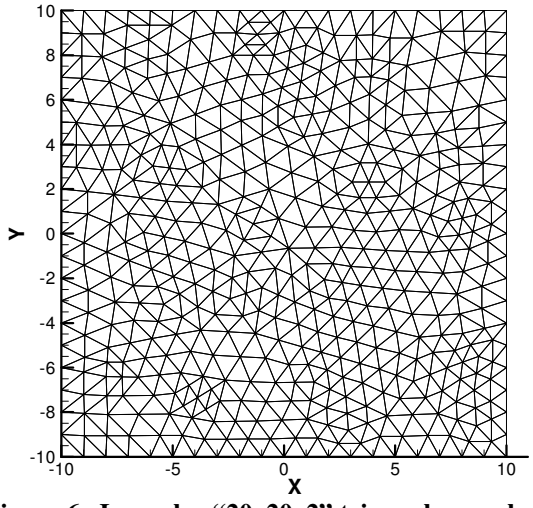

Figure 6. Irregular "20x20x2" triangular mesh.

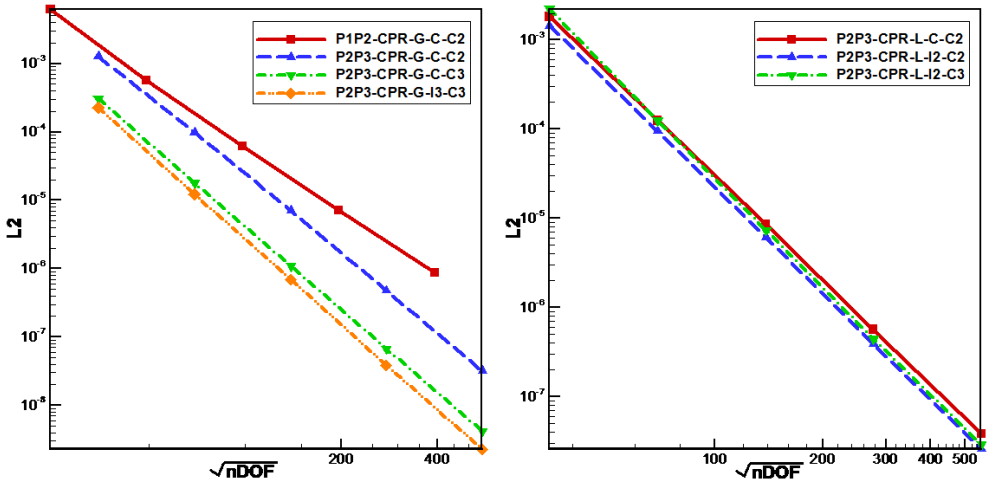

(a) Gauss points **(b) Lobatto points**

Figure 7. L_2 error of the schemes with (a) Gauss points and (b) Lobatto points for the 2D linear wave equation at t=1.

IV. Numerical Results for the Euler Equations

In this session, numeric experiments are carried out for the Euler equations for compressible flow. The two-dimensional Euler equations can be written as

$$\frac{\partial Q}{\partial t}+\frac{\partial F}{\partial x}+\frac{\partial G}{\partial y}=0\,, \tag{22}$$

where the state variables Q and inviscid flux F and G are:

$$Q=\begin{bmatrix}\rho\\ \rho u\\ \rho v\\ E\end{bmatrix}, F=\begin{bmatrix}\rho u\\ \rho u^2+p\\ \rho uv\\ u(E+p)\end{bmatrix}, G=\begin{bmatrix}\rho v\\ \rho uv\\ \rho v^2+p\\ v(E+p)\end{bmatrix} \tag{23}$$

In Eq. (23), p, u, v, ρ and E are pressure, velocity component in x and y directions, density and total energy respectively. The total energy is related to the other variables according to

$$E=\frac{p}{\gamma-1}+\frac{1}{2}\rho u^2\,. \tag{24}$$

A. Accuracy Study with Vortex Propagation Problem

In this case, we test the accuracy of the P_NP_M -*CPR* schemes for the two-dimensional Euler equations. The isotropic vortex propagation problem from Shu[29] is used. The initial condition has a mean flow of {ρ,u,v,p}={1,1,1,1} onto which an isotropic vortex is added. The isotropic vortex consists of perturbations in u, v and temperature T, but no perturbation in entropy $S=p/\rho^{\gamma}$:

$$(\delta u,\delta u)=\frac{\varepsilon}{2\pi}e^{0.5(1-r^2)}(-y,x), \tag{25}$$

$$\delta T=-\frac{(\gamma-1)\varepsilon^2}{8\gamma\pi^2}e^{1-r^2}, \tag{26}$$

$$\delta S=0, \tag{27}$$

Where $r^2=x^2+y^2$, and the vortex strength ε=5. The exact solution of this problem is just the passive convection of the isotropic vortex with the mean velocity. Figure 8. shows the density contours at different time steps.

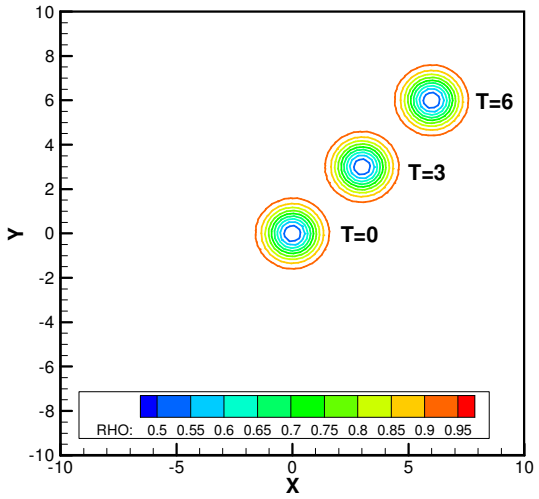

Figure 8. Density contours for the vortex propagation problem at t=0, t=3 and t=6.

In the numerical simulation, the computational domain is taken to be [-10,10]×[-10,10] with periodic boundary conditions imposed on all of the outer boundaries. As shown in Figure 6, the irregular computational meshes are used. The computation is carried out until t = 1. The L_2 error is plotted in Figure 9. and summarized in Table 3. From the simulation results, we note that the highest order of accuracy we get is 3rd at P_1P_x–*CPR* schemes and is 5th at P_2P_x–*CPR* schemes. We find that for this test case, simulations of the Lobatto points with CN correction and the Gauss points with CM correction are still more stable and accurate than those of the other combinations. Incomplete stencil seems more accurate than the complete stencil which is the same as the previous tests.

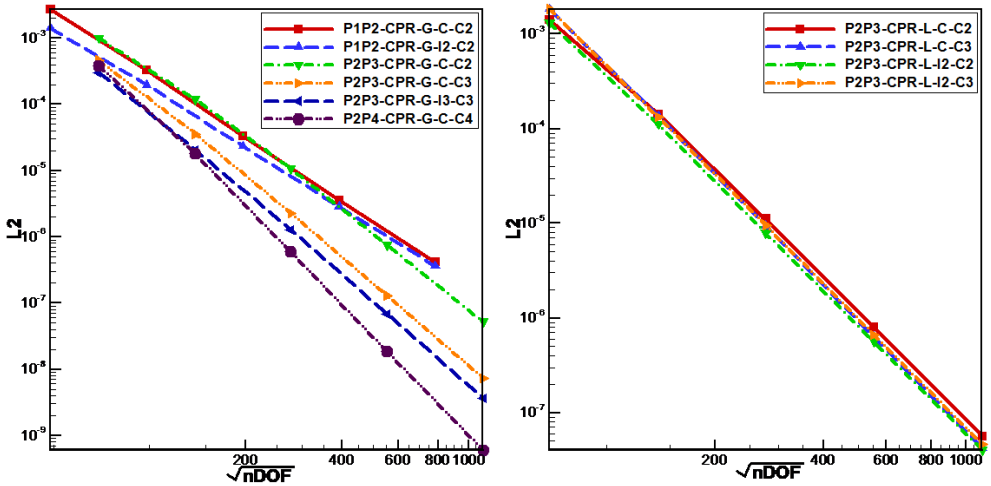

(a)Gauss points **(b) Lobatto points**

Figure 9. L_2 error of the schemes with (a) Gauss points and (b) Lobatto points for the 2D vortex propagation problem.

B. Flow in a Channel with a Smooth Bump

This internal aerodynamic problem is selected to test the order of accuracy of P_NP_M–*CPR* scheme with high-order curved boundaries. The channel has a height of 0.8 unit and a length of 3 unit. The bump is defined as

$$y = 0.0625e^{-25x^2}. \tag{28}$$

The coarsest computational mesh which has a total of 220 cells is shown in Figure 10. The smooth bump is represented with quadratic segments. Note that the mesh has mixed P1&P2 elements and the P2 elements are used

only at the wall boundary. Characteristic boundary conditions are used at both the inlet and outlet. The simulation is started from a uniform free stream with Mach number 0.5 everywhere.

Two approaches are used for the P_M reconstruction at the boundary cells. One is to use low order P_N reconstruction and the other is to perform one-sided P_M reconstruction. In order to increase the number of DOFs in the one-sided P_M reconstruction stencil, the computational grid is generated to make sure every boundary cell has at most one boundary face. The implicit lower-upper symmetric Gauss-Seidel (LU-SGS) scheme is used for time integration. The computed Mach contour of P_2P_3-*CPR-G-I3-C3* scheme is shown in Figure 11. The L_2 norms of entropy error are plotted in Figure 12. and summarized in Table 4. Because we need to use one-sided P_M reconstruction near the boundaries, only the P_NP_M-*CPR* scheme with gauss points are used for this test. From the simulation results, we note that for the P_1P_2-*CPR* scheme with P1 boundary, we get the similar order of accuracy with the P_1P_1-*CPR*. However, by using the P2 reconstruction on the internal cells the absolute entropy error is much smaller than that of P_1P_1-*CPR* scheme. Since the biggest entropy error is near the wall boundary, the one-sided P_M reconstruction on the boundary cells are needed to achieve the optimal order of accuracy for P_1P_2 and P_2P_3 CPR schemes. At the same time, we got the smallest entropy error with an incomplete P_M stencil. In order to compare the performance of the P_NP_M-*CPR* scheme with the classical CPR scheme, the P_1P_1 and P_2P_2 *CPR* results are shown in Figure 11 and Table 4 too. The results indicate that with the same degree of freedom, P_NP_M-*CPR* scheme can achieve much smaller error than the original CPR schemes.

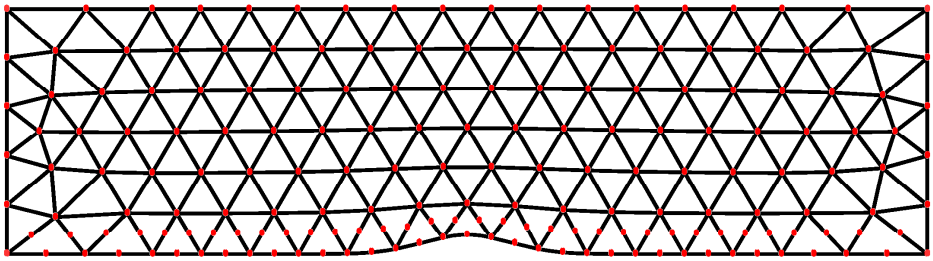

Figure 10. The coarsest triangular mesh with P2 curved boundary for the smooth bump problem.

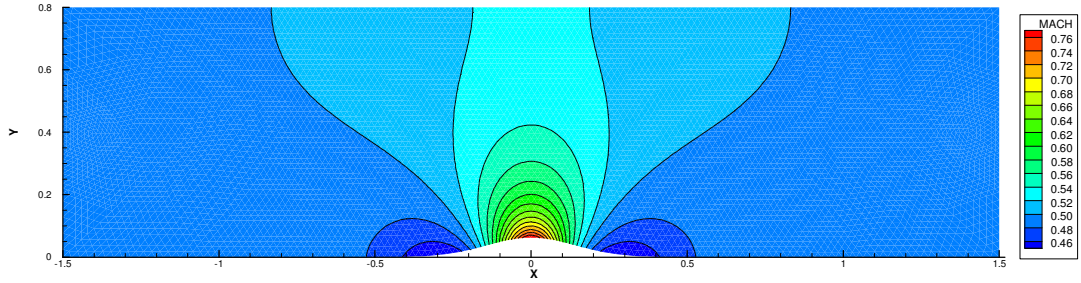

Figure 11. Mach number contour for the smooth bump problem using the P_2P_3-CPR-G-I3-C3 scheme.

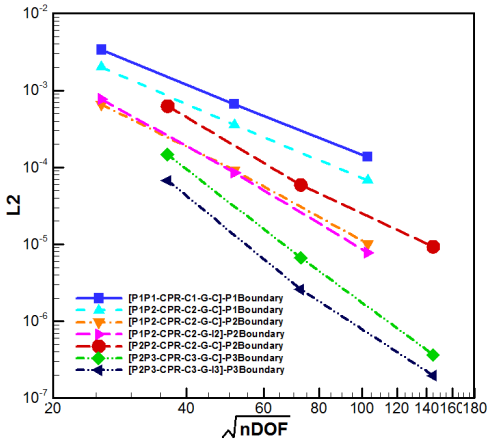

Figure 12. L_2 error for the smooth bump problem.

V. Conclusions

A $P_N P_M$-*CPR* formulation has been developed and tested in the present study. For the sake of compactness, we limit the reconstruction stencil to include the current cell and its immediate face-neighbors. The use of multiple degrees of freedom in a single cell and its neighbors opens a host of new possibilities to build schemes of various orders and different characteristics. The present formulation inherits the simplicity of the finite-difference-like CPR method, and attempts to achieve very high order of accuracy with relatively few local DOFs. In the present study, several schemes for 1D and 2D conservation laws have been developed, and evaluated in grid refinement accuracy studies. These preliminary tests indicate that the new formulation offers potential gains in accuracy, efficiency and flexibility. Possible future work will include extension to the Navier-Stokes equations.

Acknowledgments

The present research is partially supported by the Air Force Office of Scientific Research under grant FA9550-09-1-0128, National Science Foundation of China under grant 11028205, and Iowa State University.

References

[1]T.J. Barth and P.O. Frederickson, High-order solution of the Euler equations on unstructured grids using quadratic reconstruction," AIAA Paper No. 90-0013, 1990.

[2]F. Bassi and S. Rebay, High-order accurate discontinuous finite element solution of the 2D Euler equations, J. Comput. Phys. 138, 1997, pp. 251-285.

[3]F. Bassi, S. Rebay, A high-order accurate discontinuous finite element method for the numerical solution of the compressible Navier–Stokes equations. J Comp Phys, Vol. 131, No. 1, 1997, pp. 267–79.

[4]B. Cockburn and C.-W. Shu, TVB Runge-Kutta local projection discontinuous Galerkin finite element method for conservation laws II: general framework, Mathematics of Computation 52, 1989, pp. 411-435 .

[5]B. Cockburn and C.-W. Shu, The Runge-Kutta discontinuous Garlerkin method for conservation laws V: multidimensional systems, J. Comput. Phys., 141, 1998, pp. 199 - 224.

[6]B. Cockburn, C.-W. Shu, The local discontinuous Galerkin methods for time-dependent convection diffusion systems, SIAM J. Numer. Anal. Vol. 35, 1998, pp. 2440–2463.

[7]M. Dumbser, D. Balsara, E.F. Toro and C.D. Munz, A unified framework for the construction of one-step finite-volume and discontinuous Galerkin schemes, Journal of Computational Physics, Vol. 227, 2008, pp. 8209–8253

[8]Dumbser, M, PNPM schemes on unstructured meshes for time-dependent partial differential equations. In eds. Z. J. Wang, Adaptive High-order Methods in Computational Fluid Dynamics. World Scientific, Singapore, 2011, pp. 233.

[9]J.A. Ekaterinaris, High-order accurate, low numerical diffusion methods for aerodynamics, Progress in Aerospace Sciences, Vol. 41, 2005, pp. 192–300.

[10]G. J. Gassner, F. Lorcher, C-D. Munz, and J. S. Hesthaven, Polymorphic nodal elements and their application in discontinuous Galerkin methods, J. Comput. Phys., Vol. 228, 2009, pp. 1573-1590.

[11]S.K. Godunov, A finite-difference method for the numerical computation of discontinuous solutions of the equations of fluid dynamics, Mat. Sb., Vol. 47, 1959, pp. 271.

[12]S. Gottlieb, C-W. Shu, Total variation diminishing Runge–Kutta schemes. Math Comput, Vol. 67, 1998, pp. 73–85.

[13]Hesthaven J. and Warburton, T., "Nodal discontinuous Galerkin Methods", Springer, 2008.

[14]T. Haga, H. Gao and Z. J. Wang, "A High-Order Unifying Discontinuous Formulation for the Navier-Stokes Equations on 3D Mixed Grids," Math. Model. Nat. Phenom., in press.

[15]H.T. Huynh, A flux reconstruction approach to high-order schemes including discontinuous Galerkin methods, AIAA Paper 2007-4079.

[16]H.T. Huynh, A Reconstruction Approach to High-Order Schemes Including Discontinuous Galerkin for Diffusion, AIAA Paper 2009-403.

[17]Huynh, H.T., High-order methods by correction procedures using reconstructions. In eds. Z. J. Wang, Adaptive High-order Methods in Computational Fluid Dynamics, World Scientific, Singapore, 2011, pp. 422.

[18]G.E. Karniadakis, and S.J. Sherwin, Spectral-hp element methods. Oxford University Press, Oxford , 1999.

[19]D.A. Kopriva and J.H. Kolias, A conservative staggered-grid Chebyshev multidomain method for compressible flows, J. Comput. Phys., Vol. 125, 1996, pp. 244.

[20]M.-S. Liou, A sequel to AUSM, Part II: AUSM+-up for all speeds, J. Comput. Phys., Vol. 214, 2006, pp. 137–170.

[21]Y. Liu, M. Vinokur, and Z.J. Wang, Spectral (Finite) Volume Method for Conservation Laws on Unstructured Grids V: Extension to Three-Dimensional Systems, Journal of Computational Physics Vol. 212, 2006, pp. 454-472.

[22]Y. Liu, M. Vinokur, and Z.J. Wang, Discontinuous Spectral Difference Method for Conservation Laws on Unstructured Grids, Journal of Computational Physics Vol. 216, 2006, pp. 780-801.

[23]Luo, H., Luo, L., Nourgaliev, R., Mousseau, V.A., and Dinh N., A reconstructed discontinuous Galerkin method for the compressible Navier–Stokes equations on arbitrary grids, Journal of Computational Physics, Vol. 229, 2010, pp. 6961-6978.

[24]G. May and A. Jameson, A spectral difference method for the Euler and Navier-Stokes equations, AIAA paper No. 2006-304, 2006.

[25]J. Peraire and P.-O. Persson, The compact discontinuous Galerkin (CDG) method for elliptic problems, SIAM J. Sci. Comput., Vol. 30, No. 4, 2008, pp. 1806-1824.
[26]W.H. Reed and T.R. Hill, Triangular mesh methods for the neutron transport equation, Los Alamos Scientific Laboratory Report, LA-UR-73-479, 1973.
[27]P.L. Roe, Approximate Riemann solvers, parameter vectors, and difference schemes, J. Comput. Phys., Vol. 43, 1981, pp. 357-372.
[28]V.V. Rusanov, Calculation of interaction of non-steady shock waves with obstacles, J. Comput. Math. Phys. USSR 1, 1961, pp. 261-279.
[29]C.-W. Shu, "Essentially non-oscillatory and weighted essentially non-oscillatory schemes for hyperbolic conservation laws," Lecture Notes in Mathematics, Vol. 1697, 1998, pp. 325–432.
[30]K. Van den Abeele, C. Lacor, and Z. J. Wang. On the stability and accuracy of the spectral difference method. J. Sci. Comput., Vol. 37, No. 2,2008, pp. 162-188.
[31]B. van Leer, Towards the ultimate conservative difference scheme V. a second order sequel to Godunov's method, J. Comput. Phys. Vol. 32, 1979, pp. 101-136.
[32]B. Van Leer and S. Nomura, Discontinuous Galerkin for diffusion, AIAA Paper No. 2005-5108, 2005.
[33]Z.J. Wang, Spectral (Finite) volume method for conservation laws on unstructured grids: basic formulation, J. Comput. Phys. Vol. 178, 2002, pp. 210-251.
[34]Z.J. Wang, High-order methods for the Euler and Navier-Stokes equations on unstructured grids, Journal of Progress in Aerospace Sciences, Vol. 43, 2007, pp. 1-47,.
[35] Z.J. Wang, Adaptive High-Order Methods in Computational Fluid Dynamics, World Scientific Publishing, Singapore, May 2011.
[36]Z.J. Wang and H. Gao, A unifying lifting collocation penalty formulation including the discontinuous Galerkin, spectral volume/difference methods for conservation laws on mixed grids, Journal of Computational Physics, Vol. 228, 2009, pp. 8161–8186.
[37]Z.J. Wang, H. Gao and T. Haga, "A Unifying Discontinuous Formulation for Hybrid Meshes," Adaptive High-Order Methods in Computational Fluid Dynamics, Edited by Z.J. Wang, World Scientific Publishing, Singapore, 2011.
[38]Z.J. Wang, and Y. Liu, Spectral (finite) volume method for conservation laws on unstructured grids II: extension to two-dimensional scalar equation, J. Computational Physics, Vol. 179, 2002, pp. 665-697.
[39]T. Warburton, An explicit construction of interpolation nodes on the simplex, J. of Engineering Mathematics, Vol. 56, 2006, pp. 247-262.
[40]Xuan L.J. and Wu, J.Z., A weighted-integral based scheme, Journal of Computational Physics, Vol. 229, 2010, pp. 5999-6014.
[41]Zhang L., Liu W., He L., Deng X., Zhang H., A class of hybrid DG/FV methods for conservation laws II: Two-dimensional cases, J. Computational Physics, in press.

Table 1. Grid refinement Accuracy study with the 1D linear wave equation.

Scheme	No. of Cells	L_2 *error*	L_2 *order*
P_1P_3-CPR-L-C	4	1.54E-01	-
	8	1.37E-02	3.49
	16	1.37E-03	3.32
	32	1.59E-04	3.10
	64	1.95E-05	3.03
P_1P_3-CPR-G-I	4	1.89E-02	-
	8	1.46E-03	3.70
	16	1.07E-04	3.76
	32	7.13E-06	3.91
	64	4.54E-07	3.97
P_1P_5-CPR-G-C	4	2.41E-03	-
	8	6.14E-05	5.29
	16	2.18E-06	4.82
	32	7.55E-08	4.85
	64	2.50E-09	4.92
P_1P_3-CPR-G-C	4	1.56E-02	-
	8	2.17E-03	2.85
	16	2.81E-04	2.95
	32	3.39E-05	3.05
	64	3.70E-06	3.19
P_1P_4-CPR-G-C	4	2.66E-03	-
	8	2.05E-04	3.70
	16	1.62E-05	3.66
	32	1.06E-06	3.93
	64	7.04E-08	3.92
P_2P_6-CPR-L-C	4	1.26E-03	-
	8	2.22E-05	5.82
	16	3.70E-07	5.91
	32	5.95E-09	5.96
	64	9.40E-11	5.98
P_2P_4-CPR-G-I	4	1.16E-03	-
	8	2.27E-05	5.68
	16	6.12E-07	5.21
	32	1.86E-08	5.04
	64	5.84E-10	4.99
P_2P_6-CPR-G-I	4	8.97E-05	-
	8	6.92E-07	7.02
	16	8.62E-09	6.33
	32	1.37E-10	5.98
	64	2.11E-12	6.02
P_2P_8-CPR-G-C	4	7.21E-06	-
	8	1.53E-08	8.88
	16	5.02E-11	8.25
	32	2.01E-13	7.96
	64	-	-

Table 1. Continued

Scheme	No. of Cells	L_2 error	L_2 order
P_2P_6-CPR-G-C	4	1.13E-05	-
	8	2.92E-07	5.27
	16	5.75E-09	5.67
	32	9.54E-11	5.91
	64	1.68E-12	5.50

Table 2. Grid refinement Accuracy study with 2D linear wave equation.

Scheme	No. of Cells	L_2 error	L_2 order
P_1P_2-CPR-G-C-C2	10x10x2	6.28E-03	-
	20x20x2	5.63E-04	3.47
	40x40x2	6.24E-05	3.17
	80x80x2	7.15E-06	3.06
	160x160x2	8.66E-07	3.01
P_2P_3-CPR-G-C-C2	10x10x2	1.26E-03	-
	20x20x2	9.78E-05	3.69
	40x40x2	7.02E-06	3.80
	80x80x2	4.75E-07	3.89
	160x160x2	3.17E-08	3.91
P_2P_3-CPR-G-C-C3	10x10x2	3.06E-04	-
	20x20x2	1.79E-05	4.10
	40x40x2	1.09E-06	4.04
	80x80x2	6.66E-08	4.03
	160x160x2	4.16E-09	4.00
P_2P_3-CPR-G-I3-C3	10x10x2	2.26E-04	-
	20x20x2	1.22E-05	4.22
	40x40x2	6.92E-07	4.13
	80x80x2	3.85E-08	4.17
	160x160x2	2.28E-09	4.08
P_2P_3-CPR-L-C-C2	10x10x2	1.83E-03	-
	20x20x2	1.25E-04	3.88
	40x40x2	8.59E-06	3.86
	80x80x2	5.70E-07	3.91
	160x160x2	3.83E-08	3.90
P_2P_3-CPR-L-I2-C2	10x10x2	1.45E-03	-
	20x20x2	9.51E-05	3.93
	40x40x2	6.12E-06	3.96
	80x80x2	3.89E-07	3.97
	160x160x2	2.59E-08	3.91
P_2P_3-CPR-L-I2-C3	10x10x2	2.23E-03	-
	20x20x2	1.25E-04	4.16
	40x40x2	7.36E-06	4.08
	80x80x2	4.46E-07	4.05
	160x160x2	2.91E-08	3.94

Table 3. Grid refinement Accuracy study with the vortex propagation problem.

Scheme	No. of Cells	L_2 error	L_2 order
P_1P_2-CPR-G-C-C2	20x20x2	2.76E-03	-
	40x40x2	3.30E-04	2.79
	80x80x2	3.34E-05	3.06
	160x160x2	3.60E-06	3.31
	320x320x2	4.19E-07	3.21
P_1P_2-CPR-G-I2-C2	20x20x2	1.41E-03	-
	40x40x2	1.98E-04	2.83
	80x80x2	2.33E-05	3.08
	160x160x2	2.85E-06	3.04
	320x320x2	3.60E-07	2.99
P_2P_3-CPR-G-C-C2	20x20x2	1.00E-03	-
	40x40x2	1.20E-04	3.06
	80x80x2	1.07E-05	3.48
	160x160x2	7.56E-07	3.83
	320x320x2	5.19E-08	3.86
P_2P_3-CPR-G-C-C3	20x20x2	4.65E-04	-
	40x40x2	3.58E-05	3.70
	80x80x2	2.28E-06	3.98
	160x160x2	1.30E-07	4.13
	320x320x2	7.30E-09	4.16
P_2P_3-CPR-G-I3-C3	20x20x2	3.01E-04	-
	40x40x2	2.05E-05	3.88
	80x80x2	1.28E-06	4.00
	160x160x2	6.84E-08	4.22
	320x320x2	3.63E-09	4.24
P_2P_4-CPR-G-C-C4	20x20x2	3.84E-04	-
	40x40x2	1.80E-05	4.41
	80x80x2	5.94E-07	4.92
	160x160x2	1.86E-08	5.00
	320x320x2	6.00E-10	4.95
P_2P_3-CPR-L-C-C2	20x20x2	1.41E-03	-
	40x40x2	1.42E-04	3.31
	80x80x2	1.11E-05	3.67
	160x160x2	7.96E-07	3.81
	320x320x2	5.64E-08	3.82
P_2P_3-CPR-L-C-C3	20x20x2	1.83E-03	-
	40x40x2	1.36E-04	3.75
	80x80x2	9.46E-06	3.84
	160x160x2	6.33E-07	3.90
	320x320x2	4.22E-08	3.91

Table 3. Continued

Scheme	No. of Cells	L_2 error	L_2 order
P_2P_3-CPR-L-I2-C2	20x20x2	1.30E-03	-
	40x40x2	1.12E-04	3.54
	80x80x2	7.87E-06	3.83
	160x160x2	5.59E-07	3.82
	320x320x2	4.01E-08	3.80
P_2P_3-CPR-L-I2-C3	20x20x2	1.84E-03	-
	40x40x2	1.33E-04	3.80
	80x80x2	9.54E-06	3.80
	160x160x2	6.63E-07	3.85
	320x320x2	4.61E-08	3.85

Table 4. Grid refinement Accuracy study with the smooth bump problem.

Scheme	No. of Cells	L_2 error	L_2 order
P_1P_1-CPR-G-C-C1 P1 Boundary	220	3.37E-03	-
	880	6.63E-04	2.35
	3520	1.37E-04	2.28
P_1P_2-CPR-G-C-C2 P1 Boundary	220	2.01E-03	-
	880	3.56E-04	2.50
	3520	6.75E-05	2.40
P_1P_2-CPR-G-C-C2 one-sided P2 Boundary	220	6.55E-04	-
	880	9.17E-05	2.84
	3520	1.02E-05	3.16
P_1P_2-CPR-G-I2-C2 one-sided P2 Boundary	220	7.72E-04	-
	880	8.54E-05	3.18
	3520	7.82E-06	3.45
P_2P_2-CPR-G-C-C3 P2 Boundary	220	6.24E-04	-
	880	5.90E-05	3.40
	3520	9.29E-06	2.67
P_2P_3-CPR-G-C-C3 one-sided P3 Boundary	220	1.46E-04	-
	880	6.70E-06	4.45
	3520	3.67E-07	4.19
P_2P_3-CPR-G-I3-C3 one-sided P3 Boundary	220	6.74E-05	-
	880	2.60E-06	4.70
	3520	1.97E-07	3.72